MOLECULAR GAS AND DUST AT $z = 2.6$ IN SMM J14011+0252: A STRONGLY LENSED, ULTRALUMINOUS GALAXY, NOT A HUGE, MASSIVE DISK.

D. Downes

Institut de Radio Astronomie Millimétrique, Domaine Universitaire, F-38406 St. Martin d'Hères, France

P.M. Solomon

Astronomy Program, State University of New York, Stony Brook, NY 11794

ABSTRACT

We used the IRAM Interferometer to detect CO(3–2), CO(7–6), and 1.3 mm dust continuum emission from the submillimeter galaxy SMM J14011+0252 at $z = 2.6$. Contrary to a recent claim that the CO was extended over 6.6″ (57 kpc), the new data yield a size of $2'' \times \leq 0.5''$ for the CO and the dust. Although previous results placed the CO peak in a region with no visible counterpart, the new maps show the CO and dust are centered on the J1 complex seen on *K*-band and optical images. We suggest the CO is gravitationally lensed not only by the foreground cluster A1835, but also by an individual galaxy on the line of sight. Comparison of measured and intrinsic CO brightness temperatures indicates the CO size is magnified by a factor of 25 ± 5. After correcting for lensing, we derive a true CO diameter of $\sim 0.08''$ (700 pc), consistent with a compact circumnuclear disk of warm molecular gas similar to that in Arp 220. The high magnification means the true size, far-IR luminosity, star formation rate, CO luminosity, and molecular gas mass are all comparable with those in present-epoch ultraluminous IR galaxies, not with a huge, massive, early-universe galactic disk.

Subject headings: galaxies: structure – galaxies: individual (SMM J14011+0252) – galaxies: ISM – gravitational lensing – cosmology

1. EVIDENCE FOR A STARBURST IN SMM J14011+0252

In the past decade, about twenty CO sources at redshifts from $z = 2$ to 4.7 have been detected at millimeter wavelengths. Most of these high-z molecular-line emitters are

gravitationally lensed, ultraluminous infrared galaxies (ULIGs), often hosting quasars and vigorous starbursts that may dominate star formation in the early universe. One of these galaxies is SMM J14011+0252 at $z = 2.565$, originally found by Smail et al. (1998). It is located behind the galaxy cluster Abell 1835 at $z = 0.25$, and is relatively intense in the submillimeter band, with an 850 μm flux density of 15 ± 2 mJy (Ivison et al. 2000). The visible spectrum of SMM J14011+0252, taken with the Keck-II telescope, covers rest-frame wavelengths 1200–2400 Å, and has a blue continuum with weak, narrow Lyα emission and UV absorption lines of C IV, Si II/ O I, Al III, Si IV, and C II, all typical of star-forming galaxies (Ivison et al. 2000). There is no sign of highly-ionized species like N V and no broad Lyα or Hα features, so there is no evidence for emission from a central black hole accretion disk. The Hα-to-[N II] ratio is 3, as usually found in H II regions. The 21.5 cm radio flux of $\sim 100\,\mu$Jy agrees with the far-IR-radio correlation for nearby starburst galaxies (Ivison et al. 2000; 2001). All these facts indicate 14011+0252 is powered by star formation rather than a dust-shrouded quasar.

The CO(3–2) line in SMM J14011+0252 was first detected with the Caltech interferometer (Frayer et al. 1999). New results by Ivison et al. (2001) seemed to show the CO was extended over 6.6″, or 57 kpc. Even allowing for the magnification of 2.5 assumed by Ivison et al., the CO scale length would be > 20 kpc, more than twenty times larger than the CO-emitting, starburst nuclear disks in local ultraluminous IR galaxies. The huge size and CO luminosity lead to a picture of an immense protogalaxy with $\geq 10^{11}\,M_\odot$ of metal-enriched, *molecular* gas (Ivison et al. 2001). This is equal to or greater than the stellar mass of all modern spiral galaxies and is surpassed only by the baryonic mass of giant ellipticals. The existence of such a huge and massive system at $z = 2.6$ would have profound implications for theories of galaxy formation.

Ivison et al. also measured a CO centroid that did not coincide with the optical or *K*-band objects seen with the *Hubble Space Telescope (HST)* or the United Kingdom Infrared Telescope (UKIRT), thus implying that most of the large starburst region is completely hidden from view. To verify the CO extent and position, we re-observed the source at 1.3 mm and 3 mm with the IRAM Interferometer on Plateau de Bure, France. We find a much smaller source, centered on a *K*-band feature, that we believe is strongly gravitationally lensed, leading to a picture of SMM J14011+0252 as an early-universe ultraluminous galaxy with a compact star-forming disk in its center.

2. DETECTIONS, POSITIONS, AND SIZES

2.1. *Observing Technique*

The interferometer recorded data at 1.3 mm and 3 mm simultaneously, with six 15-m antennas spaced from 24 m to 330 m. The most compact array, with spacings ≤ 80 m, integrated for 24 hours in excellent weather with $\sim$2 mm of precipitable water vapor and r.m.s. phase errors of $\leq 20^\circ$ at 1.3 mm. The longer-baseline configurations had another 16 hours with 1.3 mm phase errors $\leq 40^\circ$. The SIS receivers had equivalent system temperatures outside the atmosphere of 150 K at 3 mm (97 GHz) in the lower sideband, and 250 to 400 K at 1.3 mm in upper and lower sidebands separated by 3 GHz, with the upper band at 226 GHz. The spectral correlators covered 1700 km s^{-1} at 3 mm and 800 km s^{-1} at 1.3 mm, with resolutions of 8 and 4 km s^{-1}, respectively. The amplitude calibrators were 3C273 (18.2 Jy at 3 mm and 12.9 Jy at 1.3 mm), and MWC349 (1.0 and 1.7 Jy at 3 and 1.3 mm). The uncertainties in the flux scales are $\pm$5% at 3 mm and $\pm$10% at 1.3 mm.

The observing program monitored phases every 20 min, at 3 and 1.3 mm simultaneously, on the nearby calibrators IAP 1413+135 and 1334−127, which are northeast and southwest of 14011+0252 (Table 1). The data recording routine uses the 1.3 mm total power to correct amplitudes and phases at 3 and 1.3 mm for short-term changes in atmospheric water vapor. A subsequent calibration program scales the 3 mm curve of phase vs. time to 1.3 mm, subtracts it from the observed 1.3 mm calibrator phases, and fits the phase difference between the two receivers. To all the visibilities, the calibration program assigns weights proportional to the integration time and the inverse square of system temperature. One can then make maps either with these weights ("natural weighting") or with uniform weighting of the u, v data.

2.2. *CO Lines at 3 and 1.3 mm*

We detected both CO(3–2) and CO(7–6) with good sensitivity (Figs. 1—3). The CO (3–2) flux, linewidth, and redshift all agree with the results of Frayer et al. (1999). The apparent CO(3–2) luminosity is 1×10^{11} K km s^{-1} pc^2, a very high value, well beyond the maximum of the CO power histogram for ultraluminous galaxies. For comparison, the galaxy Arp 220 has CO(1–0) and CO(3–2) luminosities of 8×10^9 K km s^{-1} pc^2, about twelve times less than 14011+0252. In the survey of 37 ultraluminous galaxies by Solomon et al. (1997), the median CO luminosity was that of Arp 220, and the dispersion was surprisingly small, only 30 per cent. In that sample, the highest CO luminosity, for the galaxy 20087−0308, was only twice as high as Arp 220's, so SMM J14011+0252 definitely appears to be off-scale.

The CO(7–6) line is a new detection. The CO $J = 7$ level is $J(J+1) \times 2.77\,\mathrm{K} = 155\,\mathrm{K}$ above the ground state, and normally is not populated in galactic spiral-arm molecular clouds, which have mean temperatures of 5 to 20 K and H_2 densities of $\sim 200\,\mathrm{cm}^{-3}$. For example, in the central 350 pc radius of our Galaxy, the CO measurements by Fixsen, Bennett, & Mather (1999) with the *Cosmic Background Explorer (COBE)*, when converted to L'_{CO} units, show CO(7–6) is weaker than CO(3–2) by a factor of 15. In the inner 4.8 kpc radius ($l \pm 32^\circ$) of the Milky Way, excluding the galactic center, the estimates by Fixsen et al. when converted to L'_{CO} units, show CO(7–6) is weaker than CO(3–2) by a factor of 160. In contrast to its low level in the Milky Way, CO(7–6) is remarkably prominent in 14011+0252, with a fifth of the CO(3–2) luminosity. As well as the relative power, the absolute values are very impressive: The apparent CO(3–2) luminosity is 250 times greater than that of the Milky Way, and the apparent CO(7–6) luminosity is 8000 times greater. The strength of CO(7–6) indicates the CO lines in 14011+0252 are emitted in gas at ~ 50 to 60 K and more importantly, at an H_2 density ~ 1700 to $2000\,\mathrm{cm}^{-3}$, i.e., ten times higher than in typical spiral-arm molecular clouds in our Galaxy.

2.3. *Dust Continuum at 1.3 mm*

We detected the 1.3 mm (224.7 GHz) continuum, in double sideband, and in the upper and lower sidebands separately. All the data subsets agree in the peak position and intensity, within the errors. The final 1.3 mm continuum map (Fig. 3b) from both sidebands, excluding CO(7–6), shows a source with a flux density of 2.5 ± 0.8 mJy ($1\,\sigma$). This is about half the value of 6.1 ± 1.5 mJy reported by Ivison et al. (2000) at 1.35 mm. The CO(7–6) does not cause this discrepancy, because the line is only 225 MHz wide, and the bandwidth of the bolometer used by Ivison et al. (>30 GHz) would dilute the line flux by a factor >100. We could reconcile their results with ours if the flux-weighted centroid of their bolometer band were at ∼1.15 mm (260 GHz) instead of 1.35 mm. With a source spectrum steeply rising as $\nu^{3.5}$, our narrow-band heterodyne measurement of 2.5 mJy at 225 GHz would correspond to a flux of 5 ± 2 mJy at 260 GHz.

At 3 mm (97.0 GHz), there is no continuum, to a limit of 0.6 mJy ($4\,\sigma$), consistent with the 1.3 mm emission being optically thin radiation by dust. For a dust spectral index of 3.5, the expected 3 mm flux density would be only 0.15 mJy, a factor of 4 below our limit.

2.4. *Position Measurement*

In the CO(3–2), (7–6), and 1.3 mm dust maps (Figs. 2 and 3), the peaks are all $\sim 1.6''$ south of the initial CO(3–2) position measured by Frayer et al. (1999), and $\sim 1.0''$ south of the revised CO position listed by Ivison et al. (2001). For identifying the CO with optical objects in the *HST* field, we must look at both the systematic and statistical uncertainties. In these data, the calibrators 1413+135 and 1334-127 are 11° and 15° away from 14011+0252. With such calibrator angles, the interferometer has an astrometric uncertainty of $\sim 0.2''$ (see Downes et al. 1999, sect.4). The system noise adds a statistical error, which for a point source is

$$\Delta\theta \approx (B/2)/(S/N) \tag{1}$$

where B is the beamwidth, and S/N is the signal-to-r.m.s.-noise ratio. With natural weighting, our CO(3–2) map has a $6''$ beam and $S/N = 24$, and with uniform-weighting (Fig. 2) it has a $3.3''$ beam and $S/N = 16$. The best of these gives a noise error $\Delta\theta = 0.10''$ r.m.s., which convolved with the astrometric error ($0.2''$) yields a root sum square (r.s.s.) error of $0.22''$. The CO(7–6) map (Fig. 3) has a $2.2''$ beam and $S/N = 9.4$ on the peak, so the noise error is $\Delta\theta = 0.12''$ r.m.s., which with the astrometric uncertainty ($0.2''$) gives an r.s.s. error of $0.23''$.

The new CO position thus differs significantly from those obtained by Frayer et al. (1999) and Ivison et al. (2001), but agrees, within the 1σ errors, with the optical position of the J1 complex as determined by Ivison et al. from the *HST* *R*-band image (Table 2 and Fig. 4). Somewhat more puzzling is the $0.8''$ difference between the centroids of the CO and the 1.4 GHz nonthermal continuum. The 1.4 GHz continuum is extended by $2''$ and is likely to come from supernovae in the starburst fueled by the molecular gas. Although their centroids need not coincide exactly, the half-power ellipse of the synchroton source, as determined by Ivison et al. (2001), actually does include the CO peak and the optical J1 component (Fig. 4). The low signal-to-noise ratio (5.5σ) on the 1.4 GHz map by Ivison et al. (2001) may cause part of the apparent discrepancy, and also explain why their new position for this VLA source differs by $1.4''$ from that in the Ivison et al. (2000) paper. If we increase the position errors to 2σ, then the 1.4 GHz and CO peaks nearly overlap. Given this uncertainty, and the $2''$ size of the 1.4 GHz continuum, the position difference between the CO peak and the nonthermal peak may be less significant than it seems at first glance.

2.5. *Size Measurement*

The previous report that the CO was extended over 6.6″ (Ivison et al. 2001) is not confirmed by fits to the visibilities in the u, v plane (Fig. 5) which give gaussian full widths to half power of $2'' \times < 0.5''$. The interferometer does not "resolve out" more extended structure, because our maps contain *all* of the CO flux reported by Frayer et al. (1999) and Ivison et al. (2001). Our most compact array has a 3 mm beam of $7'' \times 6''$, that would have responded to a 6″ source without missing any flux. This large-beam map yields the same CO flux as the small-beam map in Fig. 2. One can also think of this in the visibility plane. A 3 mm source with a size of 2.2″ drops to half flux at a projected baseline of 120 m (Fig. 5). A source three times larger would loose half its flux at a spacing three times shorter, or 40 m. Because 14011+0252 is at low declination, our interferometer has projected baselines from 16 m onward, and would have been sensitive to a 6.6″ source, had it existed. We can only speculate that the CO map by Ivison et al. (2001) may have too low a signal-to-noise ratio ($S/N \sim$5.5 near the peak) to give an accurate size. A good rule of thumb is that one needs $S/N \geq 10$ for a diameter measurement.

If the size really had been 6.6″, then even with the magnification of 2.5 assumed by Ivison et al., the CO diameter would have been an astonishing 20 kpc, more than 20 times larger than the CO-emitting regions in nearby, low-z ultraluminous IR galaxies. It would also contradict results showing that objects at $z >$2 in the Hubble Deep Fields have quite small linear dimensions (Ferguson, Dickinson, & Williams 2000). These studies show that early-universe starbursts are efficient and small, about the size of galaxy cores, not the size of complete, modern-day galactic disks. Even in the large, well-developed, gas-rich galaxy disks in the present-day universe, and even in CO(1–0), the lowest rotational transition, most of the CO is concentrated within a central radius of 3 kpc (see, e.g., the CO scale lengths in the galaxy surveys by Regan et al. 2001, their Table 4, and Nishiyama, Nakai, & Kuno 2001, their Table 2). If the CO in 14011+0252 were really as large as 6.6″, then the 2″ beam at 1.3 mm would have revealed a velocity gradient of a few hundred km s^{-1} across the source, but there is no gradient — neither in the grids of spectra (Fig. 6) nor in the maps of individual CO velocity channels (Fig. 7).

Although the CO region is not as large as originally claimed, its measured diameter of 2″ (17 kpc) is still unlikely to be a true size. Merely detecting CO(7–6) makes such a large CO extent very improbable. Because the CO J=7 level is 155 K above the ground state, seeing the line at all implies a gas kinetic temperature of at least 50 K and an average H_2 density > 1500 cm^{-3}. These temperatures and mean densities are found in the circumnuclear starburst disks of radius $\sim$ 300 pc in the centers of ULIGs, but they are implausible over 17 kpc.

One could imagine a giant, spread-out, opaque "reservoir" of gas and dust hiding several simultaneous ULIG-type starbursts, but the data suggest most of the CO flux comes from a single object: (1) a single gaussian can fit the visibility amplitudes (Fig. 5); (2) the CO channel maps (Fig. 7) have only a single component, at the same position, within the noise, at all velocities; (3) the grids of the spectra (Fig. 6) have no obvious signs of multiple velocity features. In fact, both the linewidth ($190\,\mathrm{km\,s^{-1}}$) and simple profile shape of the CO spectra (Fig. 1) resemble those in Mrk 231 ($230\,\mathrm{km\,s^{-1}}$), which has a single, circumnuclear disk of radius 460 pc (Bryant & Scoville 1996; Downes & Solomon 1998). The CO(2–1) brightness temperature in Mrk 231 is 29 K in a $0.7''$ beam, corresponding to a true brightness temperature of ~ 50 K.

3. IS SMM J14011+0252 STRONGLY LENSED?

We suspect 14011+0252 is lensed not only by the core of the foreground cluster of galaxies, but also by a galaxy along the line of sight. We estimate the magnifying factor directly from the surface brightness. Since the CO is optically thick, its brightness temperature must be comparable to the gas kinetic temperature. The CO(7–6) detection tells us the gas is warm and dense, and its strength relative to CO(3–2) indicates the gas temperature. This *intrinsic* brightness temperature, divided by $1+z$, is what one would expect if the source filled the beam. The ratio of *observed* to expected brightness temperatures is then the area filling factor in the beam. Gravitational lensing preserves brightness temperature, so from the measured CO major axis, one obtains the minor axis, and their ratio is roughly the magnifying factor. Another way to derive this is to start from the apparent CO luminosity, which is

$$L'_{\rm CO}({\rm obs}) \;=\; 363\,(S\Delta V)\,\lambda^2\,D_A^2\,(1+z) \quad , \tag{2}$$

where $(S\Delta V)$ is the integrated CO flux in $\mathrm{Jy\,km\,s^{-1}}$, λ is the redshifted wavelength in mm, and D_A is the angular diameter distance in Mpc (this is a variant of eq. [3] of Solomon, Downes, & Radford 1992). If the true geometry is a gaussian with half-power diameter d, then the magnification of the CO is

$$m_{\rm CO} \;=\; \frac{d_m}{d} \;=\; \frac{1.133\,d_m^2\,\Delta V}{L'_{\rm CO}({\rm obs})}\,f_V\,T_b \quad , \tag{3}$$

where d is the true CO diameter in pc, d_m is the magnified major axis in pc, ΔV is the linewidth in $\mathrm{km\,s^{-1}}$, $L'_{\rm CO}$ is the amplified CO(3–2) luminosity in $\mathrm{K\,km\,s^{-1}\,pc^2}$, f_V is the velocity filling factor, and T_b is the CO(3–2) rest frame brightness temperature, which the CO(3–2)/CO(7–6) ratio indicates is 35 ± 5 K (this is a version of eq. [2] of Downes, Solomon, & Radford 1995). For 14011+0252, the data imply that *if the measured CO major axis is* $2''$*,*

then the gravitational lens magnifies the CO size by a factor of 25. The flux amplification inferred from our brightness temperature argument is for the sum of all the CO emission, which could be in a single, long arc or in several multiple-image spots or arclets.

Here is another way to present this argument:

1) In many respects, the spectral energy distribution of 14011+0252 resembles closely that of Arp 220 and other local-universe ULIGs, with much of the input power being re-radiated by dust at 40 to 65 K. Because its molecular gas also appears to be heated by an extraordinary starburst, 14011+0252 should have an intrinsic CO brightness temperature comparable with Arp 220's.

2) On interferometer maps of Arp 220 (Scoville, Yun & Bryant 1997; Downes & Solomon 1998), one directly measures average CO(1–0) and (2–1) brightness temperatures of 35 K, so this is a reasonable value for the intrinsic CO brightness temperature in 14011+0252.

3) We may also *calculate* a mean CO brightness temperature of Arp 220 from its total CO luminosity, linewidth, and size, for a velocity filling factor f_V=1, i.e., a mean T_b averaged over the line profile. This mean brightness temperature is also 35 K, in agreement with the direct measurement off the Arp 220 CO maps. Again, this is the expected intrinsic mean brightness temperature for the CO in 14011+0252.

4) In 14011+0252, the $L'_{\rm CO}$ (3–2)/(7–6) ratio is 5 ± 1, corresponding to a molecular gas kinetic temperature of $\sim$ 50 to 60 K, and an H_2 density of $\sim$ 1700 to 2000 $\rm cm^{-3}$. In an escape probability model, these parameters yield a predicted CO(3–2) brightness temperature of 35 ± 5 K, confirming the brightness temperature deduced by analogy with Arp 220 and other ultraluminous galaxies.

5) Because gravitational lensing conserves surface brightness, the mean CO(3–2) brightness temperature should be 35 K, whatever the magnified size.

6) The measured major axis is $2.2'' \pm 0.4''$ (gaussian FWHP), and from the intrinsic brightness temperature, linewidth, and *apparent* CO(3–2) luminosity, the derived minor axis turns out to be $0.083'' \pm 0.015''$. The major/minor axis ratio is thus 25 ± 5, and this is how much the lens magnifies the CO size.

Here's a shortcut to this answer:

1) From the observed CO(3–2) luminosity, linewidth, and size of $2.2''$, the brightness temperature would be only 0.37 K, if the emitting area were circular. Correcting by $(1 + z)$, we would get 1.3 K for the apparent T_b at z=2.6.

2) This apparent T_b of 1.3 K is 25 ± 5 times smaller than the true T_b of 35 ± 5 K expected

from the CO line ratio and the similarity of the far-IR spectrum to Arp 220's. Again, this factor of 25 is how much the lens amplifies the CO flux.

Table 2 lists the CO and dust results for 14011+0252. We also give the true radius, gas mass, dynamical mass, and far-IR luminosity after correcting downward by a factor of 25, which we think is the combined lensing effect of an individual galaxy and the cluster ensemble. The magnifying factor would of course be lower if several different, simultaneous, ULIG-level starburst sources gave area and velocity filling factors that diluted the brightness temperature in the beam. For the reasons given in sect. 2.5 — simple gaussian visibility function, one sole component in channel maps, one sole gaussian spectral profile — we prefer to treat the CO flux as coming from a single object.

4. A NEW INTERPRETATION

The CO brightness argument for strong lensing now suggests a different origin for some of the IR/optical features found by Ivison et al. (2001). Rather than being interacting galaxies and tidal tails of a merger, some of these bright knots may instead be multiple images. If for example, the J1(southeast) and J2 components are really the same object, this would explain:

— why J1 and J2 have identical redshifts in Lyα, and why they also have the same UV absorption lines;

— why J1 and J2 *both* have Lyα shifted by $-400\,\mathrm{km\,s^{-1}}$ from the lower-excitation Hα and the CO. Ivison et al. (2000; 2001) interpret J1 and J2 as interacting galaxies, and the $400\,\mathrm{km\,s^{-1}}$ shift as an outflow. But Lyα is at the *same* velocity in both J1 and J2. Why would two interacting galaxies both have a blueshifted outflow? And why would the two outflow velocity vectors be at the same angle to the line of sight so as to yield a shift of $400\,\mathrm{km\,s^{-1}}$ in both galaxies?

— why J2 looks like an arc in the high-resolution *HST* picture (Ivison et al. 2001, their Fig. 1, middle).

— why the colors of J1 and J2 are different on the low-resolution UKIRT+*HST* composite picture (Ivison et al. 2001, their Fig. 1, left): — the simplest answer is that the main blob in the J1 complex is the lensing galaxy, and it is redder than 14011+0252.

Different intrinsic *areas* at the emitted wavelengths may explain part of the different colors of J1, J2, and J1n. The observed *K*-band is rest-frame 6000 Å, including starlight from the nuclear bulge and Hα+[N II] from H II regions. The observed *U*-band is rest-frame

1000 Å, which comes from the more extincted, and possibly more confined, hot-star continuum and Lyα outflow. These different-sized regions would have different magnifications in the main and secondary images. Color differences among main and counter-images, or between arcs and bright spots, are known in other objects, such as MG 0414+0534 (Lawrence et al. 1995; Falco, Lehár, & Shapiro 1997).

In fact, the *HST* image of 14011+0252 in Fig. 8, left (from Ivison et al. 2001, their Fig. 1, middle) resembles that of the quasar MG 0414+0534 in Fig. 8, right (from Falco et al.), which has four bright spots in the "classic" lensed configuration of a bright, close double A1+A2 separated by 0.4″, plus two fainter spots B and C, each 2″ from A1+A2 and from each other (e.g., Falco et al.; Blandford & Narayan 1992, their Fig. 6c,d). As in 0414+0534, the central blob in the J1 component of 14011+0252 may actually be the lensing galaxy, and it is this galaxy that may cause the color difference between J1 and J2 on the smoothed "true color" picture by Ivison et al. (2001; their Fig. 1, left). Besides the possibly analogous quadruple spots or arclets in the optical, there are other points in common. Like 14011+0252, the galaxy 0414+0535 is at redshift 2.6, has Hα and Hβ, is very dusty and red, with $r-K = 7$ mag (e.g., Hewitt et al. 1992; Lawrence et al. 1995), and has a CO(3–2) power (Barvainis et al. 1998) identical to that of 14011+0252. The source 0414+0534 has a quasar, and we think its strong CO line comes from the same kind of circumnuclear, molecular-gas disk as in local-universe ULIGs containing quasars, like Mrk 231.

The CO in 14011+0252 may also be like the arcs #384/468 lensed by the $z = 0.175$ galaxy cluster A2218 (Pelló et al. 1988; 1992; Kneib et al. 1996). The remarkable arc #384 stretches over 4″ and appears to be two ionized regions distorted into long parallel tracks, each about 0.25″ wide. The arc is at $z = 2.515$, and its R-band flux is amplified by 2.9 ± 0.3 mag (Ebbels et al. 1996), or a factor of 14.5 ± 2. That is, the length, redshift, and magnification of the arc #384 in A2218 all resemble those of the CO in 14011+0252.

Figure 9 shows a type of model that may explain 14011+0252. In the source plane, the radial and tangential caustics are not centered on the lensing galaxy, but are pulled off-center by the mass of the $z = 0.25$ cluster Abell 1835, whose dominant cD galaxy is 50″ to the northwest. In the model, the galaxy 14011+0252 at $z = 2.6$ has a compact UV core with a diameter of 0.02″ (black core in Fig. 9, left), surrounded by a larger molecular ring (grey halo in the Figure). The core UV light is deflected into two small arcs (the black central parts of the arcs in Fig. 9, right), suggestive of the J1-SE and J2 components in the *HST* R-band field of 14011+0252. In lens plane, the millimeter CO and dust radiation is elongated into the larger grey parts of the arcs in Fig. 9. Most of the CO and dust signal is in the larger eastern arc, which we associate with J1. For the figure, we did not try to find the best model, but simply adopted a velocity width of 200 km s^{-1} and ellipticity of 0.2 for the core of the

lensing galaxy to illustrate what may be happening. More sensitive, higher-resolution CO maps are needed to derive the relative deflecting strengths of the main lensing galaxy and the cluster as a whole.

Table 3 lists the observed and de-magnified CO parameters of 14011+0252 and 0414+0534. For 0414+0535, we used the CO(3–2) data of Barvainis et al. We also give the values for Arp 220, if moved to $z = 2.6$, based on the CO(3–2) intensity (Mauersberger et al. 1999) and interferometer size measurements (Downes & Solomon 1998). The table shows that with our model of comparable CO brightness temperatures and hence strong lensing, the intrinsic properties of the molecular disks in 14011+0252 and 0414+0535 must be roughly similar to those in Arp 220 and other ultraluminous IR galaxies in the local universe.

Strong lensing may also explain another curiosity about this galaxy. Adelberger & Steidel (2000) showed 14011+0252 obeys nicely the rest-frame UV, sub-mm, and cm-radio correlations established for rapidly star-forming galaxies at low redshifts. None of the ∼800 spectroscopically confirmed $z \sim 3$ galaxies in their UV-selected sample, however, is as bright in the near-IR as 14011+0252 (R-magnitude 21.25) and $\sim 95\%$ of the galaxies in their sample are ten times fainter, implying dust fluxes ten times lower than SMMJ14011's, or ≤ 1 mJy at 850 μm. Most of their UV-selected galaxies would thus be undetectable at 1.3 mm in either the dust continuum or in CO. Our interpretation that the lens magnifies the source by more than an order of magnitude means that 14011+0252 is basically the same type of dusty, rapidly star-forming galaxy as many of the other UV-selected galaxies at high redshift.

5. CONCLUSIONS

Contrary to an apparent result that the CO in 14011+0252 is extended by 6.6″, suggesting a starburst on a much larger scale than in local ultraluminous IR galaxies, new interferometer measurents yield a size of only $2'' \times \leq 0.5''$ for the CO and dust emission. Our brightness-temperature argument further indicates the CO size must be magnified by a factor of 25. The gravitational lens may be an isolated galaxy along the line of sight, whose effects add to those of the foreground cluster A1835.

The image configuration in 14011+0252 resembles that in the gravitationally lensed quasar 0414+0535, and the circumnuclear starburst disks in both galaxies are probably magnified by comparable amounts. This means the true radii, gas masses, star formation rates, and far-IR luminosities of their molecular disks are all about the same as those in local-universe ultraluminous IR galaxies like Arp 220. They are not huge, very massive disks in the early universe.

We thank the operators on Plateau de Bure for their help in observing, R. Lucas for his aid with the visibility plots, M. Bremer for help with the figures, R. Neri for the lens model, and the referee for very useful comments.

REFERENCES

[]Adelberger, K.L., & Steidel, C.C. 2000, ApJ, 544, 218

[]Barvainis, R., Alloin, D., Guilloteau, S., & Antonucci, R. 1998, ApJ, 492, L13

[]Barvainis, R., & Ivison, R. 2002, ApJ, 571, 712

[]Blandford, R.D., & Narayan, R. 1992, ARA&A, 30, 311

[]Bryant, P.M., & Scoville, N.Z. 1996, ApJ, 457, 678

[]Downes, D., Solomon, P.M., & Radford, S.J.E. 1995, ApJ, 453, L65

[]Downes, D., & Solomon, P.M., 1998, ApJ, 507, 615

[]Downes, D., et al. 1999, A&A, 347, 809

[]Ebbels, T.M.D., Le Borgne, J.-F., Pelló, R., Ellis, R.S., Kneib, J.-P., Smail, I., & Sanahuja, B. 1996, MNRAS, 281, L75

[]Falco, E.E., Lehár, J., & Shapiro, I.I. 1997, AJ, 113, 540

[]Ferguson, H.C., Dickinson, M., & Williams, R. 2000, ARA&A, 38, 667

[]Fixsen, D.J., Bennett, C.L., & Mather, J.C. 1999, ApJ, 526, 207

[]Frayer, D.T., Ivison, R.J., Scoville, N.Z., Evans, A.S., Yun, M.S., Smail, I., Barger, A.J., Blain, A.W., & Kneib, J.-P. 1999, ApJ, 514, L13

[]Hewitt, J.N., Turner, E.L, Lawrence, C.R., Schneider, D.P., & Brody, J.P. 1992, AJ, 104, 968

[]Ivison, R.J., Smail, I., Barger, A.J., Kneib, J.-P., Blain, A.W., Owen, F.N., Kerr, T.H., & Cowie, L.L. 2000, MNRAS, 315, 209

[]Ivison, R.J., Smail, I., Frayer, D.T., Kneib, J.-P., & Blain, A.W. 2001, ApJ, 561, L45

[]Kneib, J.-P., Ellis, R.S., Smail, I., Couch, W.J., & Sharples, R.M. 1996, ApJ, 471, 643

[]Lawrence, C.R., Elston, R., Januzzi, B.T., & Turner, E.L. 1995, AJ, 110, 2570

[]Ma, C., Arias, E.F., Eubanks, T.M., Fey, A.L., Gontier, A.-M., Jacobs, C.S., Sovers, O.J., Archinal, B.A., & Charlot, P. 1998, AJ, 116, 516

[]Mauersberger, R., Henkel, C., Walsh, W., & Schulz, A. 1999, A&A, 341, 256

[]Nishiyama, K., Nakai, N., & Kuno, N. 2001, PASJ, 53, 757

[]Pelló, R., Soucail, G., Sanahuja, B., Mathez, G., & Ojero, E. 1988, A&A, 190, L11

[]Pelló, R., Le Borgne, J.F., Sanahuja, B., Mathez, G., & Fort, B. 1992, A&A, 266, 6

[]Regan, M.W., Thornley, M.D., Helfer, T.T., Sheth, K., Wong, T., Vogel, S.N., Blitz, L., & Bock, D.C.-J. 2001, ApJ, 561, 218

[]Scoville, N.Z., Yun, M.S., & Bryant, P.M. 1997, ApJ, 484, 702

[]Smail, I., Ivison, R.J., Blain, A.W., & Kneib, J.-P. 1998, ApJ, 507, L21.

[]Solomon, P.M., Downes, D., & Radford, S.J.E. 1992, ApJ, 398, L29

[]Solomon, P.M., Downes, D., Radford, S.J.E., & Barrett, J.W., 1997, ApJ, 478, 144

AAS LaTeX macros v5.0.

Table 1. POSITION MEASUREMENTS

Source	R.A. (J2000)	Decl. (J2000)	Refs. [a]
SMM J14011+0252:			
Millimeter data:			
CO(3–2)	$14^{\rm h}01^{\rm m}04.93^{\rm s} \pm 0.02^{\rm s}$	$02^\circ52'24.1'' \pm 0.2''$	1
CO(7–6)	$14^{\rm h}01^{\rm m}04.92^{\rm s} \pm 0.02^{\rm s}$	$02^\circ52'23.8'' \pm 0.3''$	1
1.3 mm dust	$14^{\rm h}01^{\rm m}04.93^{\rm s} \pm 0.03^{\rm s}$	$02^\circ52'24.5'' \pm 0.5''$	1
IR and centimeter data:			
I-band, J1 component	$14^{\rm h}01^{\rm m}04.95^{\rm s} \pm 0.02^{\rm s}$	$02^\circ52'24.0'' \pm 0.3''$	2
1.4 GHz VLA peak	$14^{\rm h}01^{\rm m}04.92^{\rm s} \pm 0.01^{\rm s}$	$02^\circ52'24.8'' \pm 0.2''$	2
Phase calibrators:			
1413+135	$14^{\rm h}15^{\rm m}58.81749^{\rm s} \pm 0.00009^{\rm s}$	$+13^\circ20'23.713'' \pm 0.003''$	3
1334−127	$13^{\rm h}37^{\rm m}39.78278^{\rm s} \pm 0.00005^{\rm s}$	$-12^\circ57'24.693'' \pm 0.001''$	3

[a] *References*: (1) This paper; (2) Ivison et al. (2001); (3) Ma et al. (1998).

Table 2. CO LINE AND DUST PROPERTIES OF SMM J14011+0252

Parameter	CO(3–2)	CO(7–6)	
Observed CO quantities:			*Unit*
Center frequency	96.989	226.251	GHz
Redshift (lsr)	2.5652 ± 0.0001	2.5651 ± 0.0002	—
CO peak flux [a]	13.2 ± 1	12.4 ± 3	mJy
Linewidth	190 ± 11	170 ± 30	$\mathrm{km\,s^{-1}}$
CO integrated flux	2.8 ± 0.3	3.2 ± 0.5	$\mathrm{Jy\,km\,s^{-1}}$
Apparent $L'_{\rm CO}$	10.8 ± 1	2.3 ± 0.3	$10^{10}\,\mathrm{K\,km\,s^{-1}\,pc^2}$
L' ratio (3–2)/(7–6)	4.8 ± 1	—	—
Major axis FWHP	2.2 ± 0.4	2.3 ± 0.5	arcsec
Minor axis FWHP	< 0.5	< 0.8	arcsec
Position angle	10 ± 20	0 ± 30	deg
Derived CO quantities: [b]			
Intrinsic CO T_b	35 ± 5	7 ± 1	K
Lens magnification	25 ± 5	23 ± 5	—
True $L'_{\rm CO}$	4.4 ± 0.9	1.0 ± 0.3	$10^9\,\mathrm{K\,km\,s^{-1}\,pc^2}$
Gas mass $M(\mathrm{H_2{+}He})$ [c]	3.5 ± 0.7	—	$10^9\,\mathrm{M_\odot}$
True radius, R	360 ± 100	420 ± 130	pc
Dynamical mass $RV^2_{\rm rot}/G$ [d]	6 ± 2	—	$10^9\,\mathrm{M_\odot}$
Dust quantities:			
Dust flux	< 0.6 $(4\,\sigma)$	2.5 ± 0.8	mJy
Dust mass	—	0.6—2.4	$10^7\,\mathrm{M_\odot}$
True $L_{\rm FIR}$	—	9 ± 3	$10^{11}\,\mathrm{L_\odot}$

[a] CO peak fluxes are for beams of $7.1'' \times 5.6''$ at CO(3–2) and $2.2'' \times 2.0''$ at CO(7–6).

[b] Adopted luminosity distance = 22.6 Gpc (H_0 =65 $\mathrm{km\,s^{-1}\,Mpc^{-1}}$, $\Omega_m = 0.3$, $\Omega_\Lambda = 0.7$); angular diameter distance = 1.781 Gpc; linear scale: $1'' \leftrightarrow 8635$ pc.

[c] Gas mass = $\pi R^2 n(H_2) 1.36 m(H_2) \Delta z$, where we took a mean H_2 number density of $2000\,\mathrm{cm^{-3}}$ in a disk of true radius R and height Δz of 50 pc. This gives a ratio $M_{\rm gas}/L'_{\rm CO} \approx 0.8\,\mathrm{M_\odot}\,(\mathrm{K\,km\,s^{-1}\,pc^2})^{-1}$, as deduced for the centers of ULIGs (Downes & Solomon 1998).

[d] For the dynamical mass within radius R, we assumed a disk inclined at 50°, rotating at $250\,\mathrm{km\,s^{-1}}$.

Table 3. SOURCE COMPARISON, FOR $z = 2.6$

Source: [a]	SMM J14011 +0252	MG 0414 +0534	Arp 220 moved to z=2.6	
Observed Line:	CO(3–2)	CO(3–2)	CO(3–2)	*Unit*
Redshift (lsr)	2.5653	2.639	2.6	—
Peak flux density	13	4.4	0.2	mJy
Linewidth	190	580	480	$\mathrm{km\,s^{-1}}$
Integrated flux	2.7	2.6	0.2	$\mathrm{Jy\,km\,s^{-1}}$
Major axis	2.2	(1.1)	0.09	arcsec
Minor axis	< 0.5	< 1.1	0.03	arcsec
Apparent $L'_{\rm CO}$	108	100	8	$10^9\,\mathrm{K\,km\,s^{-1}\,pc^2}$
Derived CO quantities:				
CO magnification	25	(20)	1	—
True radius, R	360	(235)	400	pc
True $L'_{\rm CO}$	4.4	5.0	8	$10^9\,\mathrm{K\,km\,s^{-1}\,pc^2}$
Dynamical mass $M_{\rm dyn}$ [b]	6	5.9	10	$10^9\,\mathrm{M_\odot}$
Gas mass $M_{\rm gas}$ [c]	3.5	1.1	5.0	$10^9\,\mathrm{M_\odot}$
$M_{\rm gas}\ /L'_{\rm CO}$	0.8	0.2	0.6	—
Dust quantities:				
1.3 mm flux density	2.5	20.7 nt	0.4	mJy
Apparent $L_{\rm FIR}$	23	—	1.5	$10^{12}\,\mathrm{L_\odot}$
True $L_{\rm FIR}$	1.7	—	1.5	$10^{12}\,\mathrm{L_\odot}$

[a] For SMM J14011, parameter uncertainties are listed in Table 2. For MG 0414, the data are from Barvainis et al. 1998, and the adopted magnification from Barvainis & Ivison 2002. The 1.3 mm continuum of MG 0414 is nonthermal (nt), not dust.

[b] For $M_{\rm dyn}(< R)$, the adopted rotation velocities ($\mathrm{km\,s^{-1}}$) and inclinations are (250 50°), (330, 80°), and (330, 40°).

[c] $M_{\rm gas}$ is for H_2+He, a disk height =50 pc, and $n(H_2)$ =2000 $\mathrm{cm^{-3}}$.

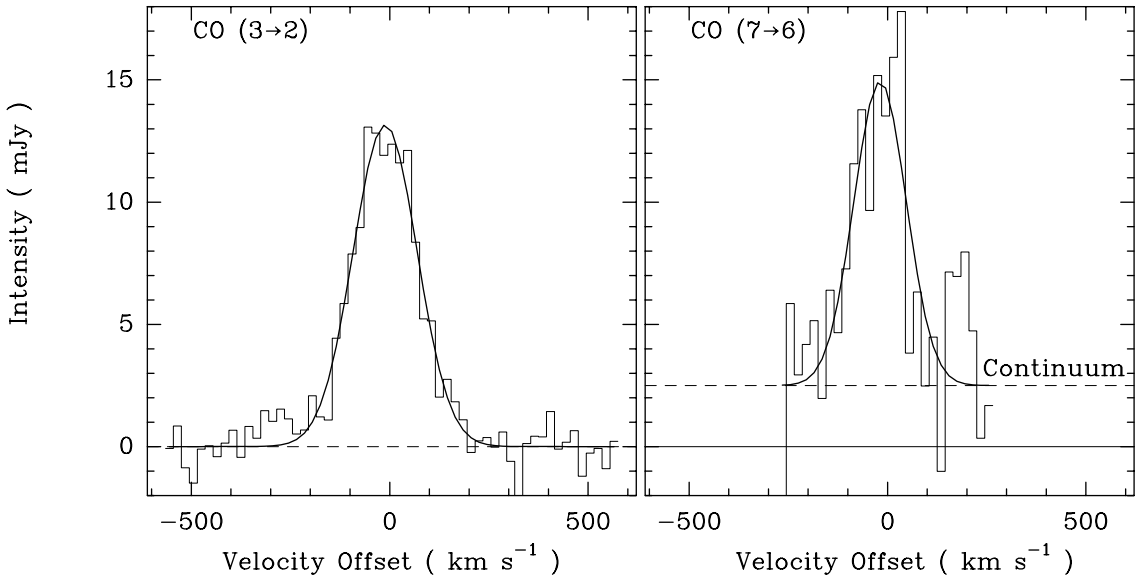

Fig. 1.— CO spectra with 20 km s^{-1} resolution, at the peak position (Table 1) of SMM J14011+0252, with their gaussian fit curves superposed.
Left: CO(3–2) spectrum. The r.m.s. noise is 0.84 mJy, and the beam is $7.1'' \times 5.6''$ with T_b/S = 3.3 K/Jy. The line peak is 13.2 mJy, or 0.043 K. Velocity offsets are relative to 96.989 GHz. *Right:* CO(7–6) spectrum. The r.m.s. noise is 3.1 mJy, and the beam is $2.2'' \times 2.0''$ with $T_b/S = 5.4$ K/Jy. Velocity offsets are relative to 226.251 GHz. The line is above a 2.5 mJy continuum (measured in the other sideband).

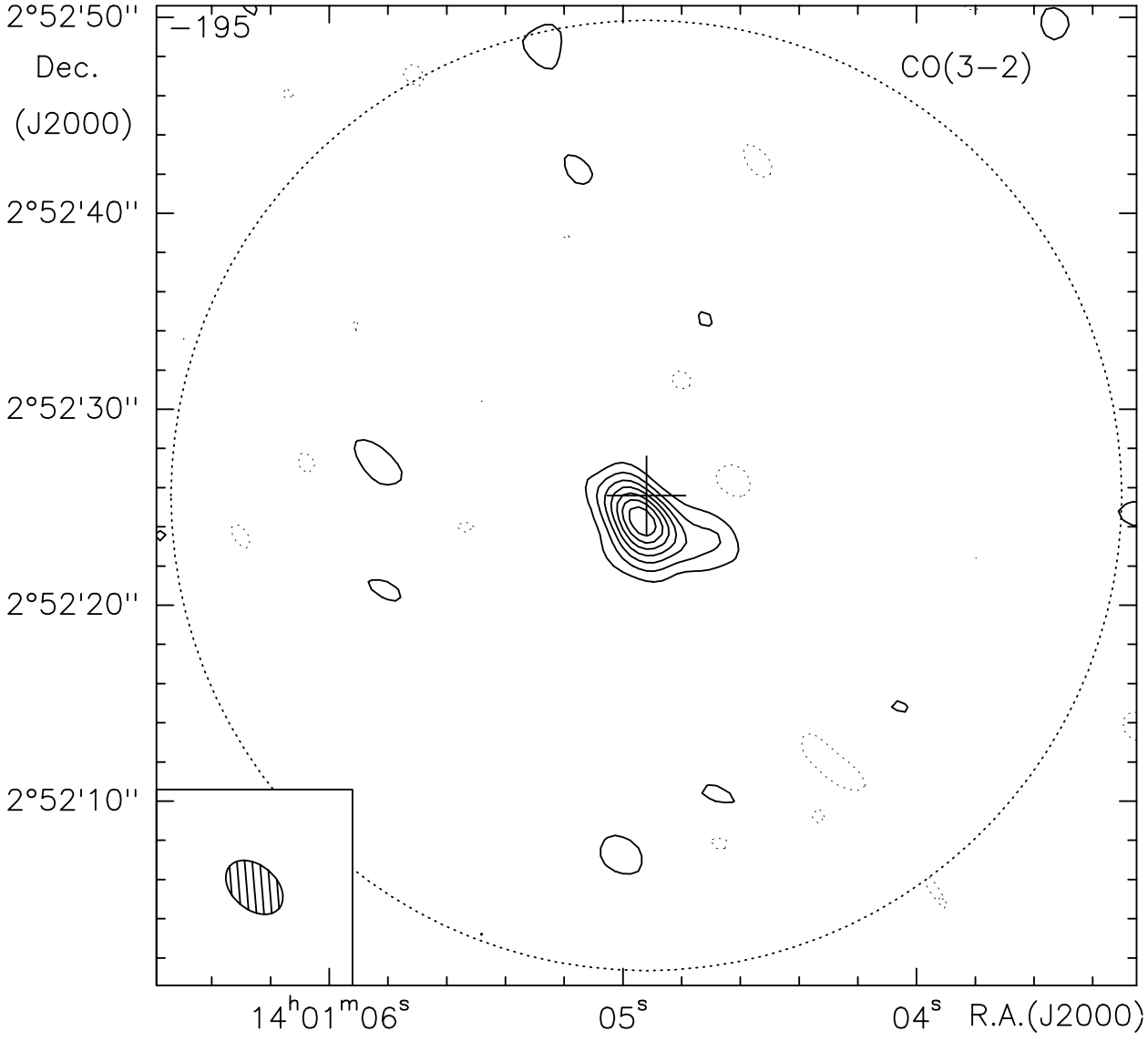

Fig. 2.— Map of CO(3–2) integrated over 260 km s^{-1}, from SMM J1401+0252. The beam is $3.3'' \times 2.3''$ at p.a. 50° (lower left), with $T_b/S = 17.2$ K/Jy. The large dotted circle shows the $49''$ primary lobe. The contour step is 0.82 mJy beam^{-1} (2σ), or 0.21 Jy beam^{-1} km s^{-1} in velocity-integrated flux; negative contours are dashed, zero level omitted. The cross marks the initial CO position (Frayer et al. 1999), that we adopted as the phase center for our observing.

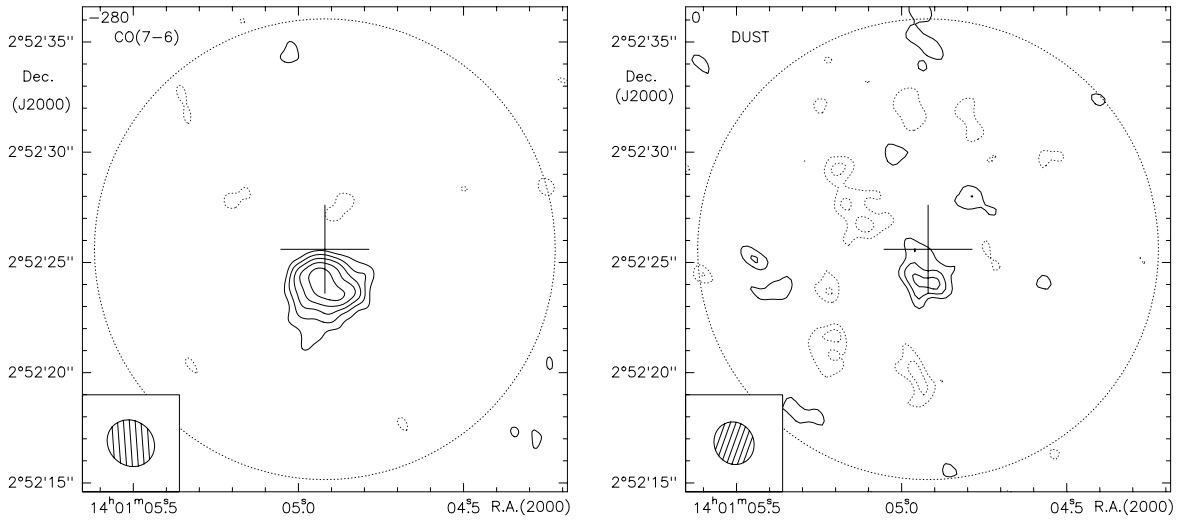

Fig. 3.— Maps of CO and dust at 1.3 mm.
Left: CO(7–6) integrated over the central 160 km s^{-1} of the profile. Contours start at 2.6 mJy beam^{-1} (2σ) and increase in steps of 1.3 mJy beam^{-1} (1σ), or a step in velocity-integrated flux of 0.21 Jy beam^{-1} km s^{-1}; negative contours are dashed, zero level omitted. On this map, the continuum peak of 1.6 mJy would be below the first contour. The beam is $2.2'' \times 2.0''$ at p.a. 48° (lower left), with $T_b/S = 5.4$ K/Jy.
Right: Dust continuum at 1.3 mm (224.7 GHz). Contours start at 0.8 mJy beam^{-1} ($2\,\sigma$) and increase in steps of 0.4 mJy ($1\,\sigma$); negative contours are dashed, zero level omitted. The spatially-integrated flux density is 2.5 mJy. The beam is $2.0'' \times 1.8''$ at p.a. 25° (lower left), with $T_b/S = 6.7$ K/Jy. In each diagram, the large dotted circle shows the $20.9''$ primary lobe, and the cross marks the initial CO position from Frayer et al. (1999).

Fig. 4.— CO contours superposed on the *HST* F702W image from Ivison et al. (2001), and compared with VLA halfwidth at 1.4 GHz.
Left: CO(3–2) map, with same contours as in Fig. 2, beam $3.3'' \times 2.3''$ at p.a. 50°.
Right: CO(7–6) map, with same contours as in Fig. 3a, beam $2.2 \times 2.0''$ at p.a.48°.
In each diagram, the dark ellipse shows the $2.3'' \times 1.5''$ half-power widths of the 1.4 GHz non-thermal VLA source, as derived by Ivison et al. (2001). The 1-σ error quoted by those authors for the optical position is $\pm 0.3''$ (small circle above the F702W label).

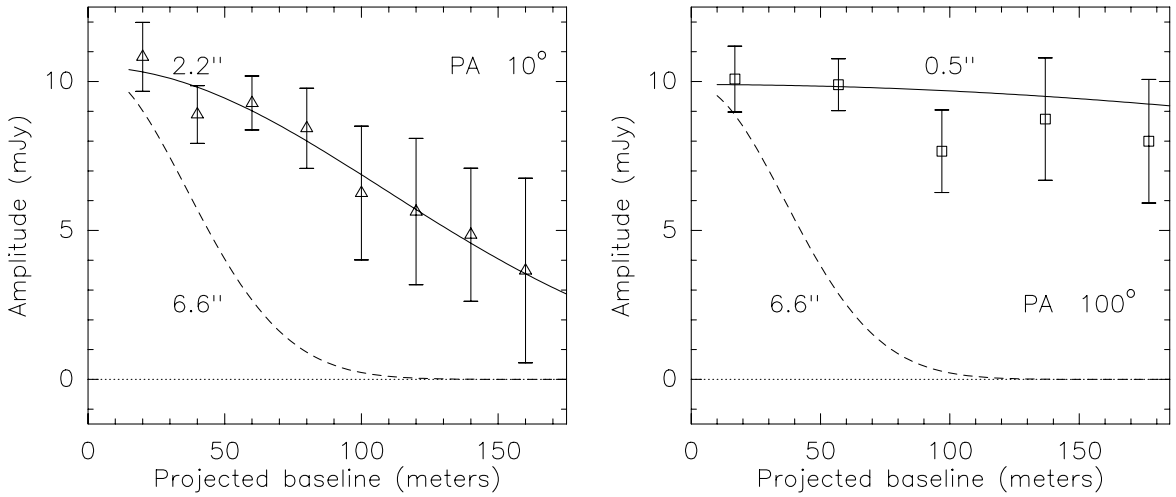

Fig. 5.— Size measurement: CO(3–2) visibility amplitudes north-south and east-west. The solid curves are the best fits for an elliptical gaussian with half-power widths $2.2'' \times \leq 0.5''$, at p.a. 10° on the sky. The dashed curves show where the amplitude would have fallen if the source size had been 6.6″. *Left:* Visibility ∼ north-south (p.a. 10°), averaging step 20 m. *Right:* Visibility ∼ east-west (p.a. 100°), averaging step 40 m. For both figures, the CO profile was integrated over $260\,\mathrm{km\,s^{-1}}$, centered on the CO peak of SMM J14011+0252. Error bars are 1-σ.

Fig. 6.— CO spectra with $20\,\mathrm{km\,s^{-1}}$ resolution, on grids around CO the peak of SMM J14011+0252.
Left: CO(3–2) spectra with a grid spacing of $2''$. The beam is $5.9'' \times 4.5''$, with $T_b/S = 4.9\,\mathrm{K/Jy}$, and the r.m.s. noise is 0.8 mJy. Velocity offsets are relative to 96.989 GHz.
Right: CO(7–6) spectra with a grid spacing of $1''$. The beam is $2.2'' \times 2.0''$ with $T_b/S = 5.4\,\mathrm{K/Jy}$, and the r.m.s. noise is 3.1 mJy. Velocity offsets are relative to 226.251 GHz.

Fig. 7.— CO channel maps of SMM J14011+0252.
Left: CO(3–2) in $20\,\mathrm{km\,s^{-1}}$ channels with a $5.9'' \times 4.5''$ beam (lower right box), with $T_b/S = 4.9\,\mathrm{K/Jy}$. Contour steps are 1.6 mJy (2σ). Velocity offsets (upper left corners) are relative to 96.989 GHz.
Right: CO(7–6) in $40\,\mathrm{km\,s^{-1}}$ channels with a $2.2'' \times 2.0''$ beam (lower right box), with $T_b/S = 5.4\,\mathrm{K/Jy}$. Contours start at 4.4 mJy (2σ), and increase in steps of 2.2 mJy (1σ). Velocity offsets (upper left corners) are relative to 226.251 GHz. In all diagrams, the cross marks the initial CO position from Frayer et al. (1999).

Fig. 8.— Comparison of *HST* images of SMM J14011+0252 and MG 0414+0534.
Left: *HST* *R*-band field of SMM J14011+0252, covering 6.0″ on a side, with tick marks every 1″ (from Ivison et al. 2001). The labels give our interpretation of the objects as lensing galaxy, close double J1-southeast, and two counter-images.
Right: *HST* *I*-band exposure of MG 0414+0534, covering 5.8″ on a side (from Falco et al. 1997). We mark the lensing galaxy, the close double A1+A2 and the two counter-images B and C. In the model of Falco et al., the four spots are the quasar, while the arc is a distorted view of a much larger ionized region, about 200 pc from the quasar.

Fig. 9.— A model that may explain SMM J14011+0252.
Left: Source plane. The lensing galaxy is at (0,0), the radial caustic (outer ellipse) and the tangential caustic (inner diamond) are pulled off-center by the mass of the $z = 0.25$ cluster Abell 1835, which is centered at ($-40''$, $+20''$). The background ultraluminous galaxy at $z = 2.565$ has a compact UV core with a diameter of $0.02''$ (black core), surrounded by a larger ring of molecular gas with a diameter of $0.18''$ (grey halo).
Right: Lens Plane. The lensing galaxy is at (0,0), the outer ellipse is the tangential critical curve and the inner ellipse is the radial critical curve, corresponding to the caustics in the source plane. The core UV light of the background galaxy is deflected into small arclets (the black central parts of the arcs), similar to the J1-southeast double and the J2 and J1n components in the *HST R*-band field of 14011+0252. The millimeter CO and dust radiation is distorted into the larger grey arcs. Most of the CO and dust flux is in the large arc, associated with the J1 component.